Journal of Macromolecular Science, Part A
Publication details, including instructions for authors and subscription information:
http://www.informaworld.com/smpp/title~content=t713597274

Solvothermal Synthesis of Calcium Phosphate Nanowires Under Different pH Conditions

Kun Wei[a]; Chen Lai[a]; Yingjun Wang[a]
[a] Key Laboratory of Specially Function Materials and Advanced Manufacturing Technology of Ministry of Education, South China University of Technology, Guangzhou, China

To cite this Article Wei, Kun , Lai, Chen and Wang, Yingjun(2006) 'Solvothermal Synthesis of Calcium Phosphate Nanowires Under Different pH Conditions', Journal of Macromolecular Science, Part A, 43: 10, 1531 — 1540
To link to this Article: DOI: 10.1080/10601320600896785
URL: http://dx.doi.org/10.1080/10601320600896785

Journal of Macromolecular Science®, Part A: Pure and Applied Chemistry, 43:1531–1540, 2006

ISSN 1060-1325 print/1520-5738 online
DOI: 10.1080/10601320600896785

Solvothermal Synthesis of Calcium Phosphate Nanowires Under Different pH Conditions

KUN WEI, CHEN LAI, AND YINGJUN WANG

Key Laboratory of Specially Function Materials and Advanced Manufacturing Technology of Ministry of Education, South China University of Technology, Guangzhou, China

Nano-size calcium phosphate is prepared via solvothermal synthesis methods, using a reverse micelles solution. The influence of pH value on the crystallinity, morphology, and composition of the nanoparticles are investigated. It was found that the crystallinity increased as pH increased. However, notable changes in the morphology of the final products can be observed. At pH 6.0, long nanowires (800 nm long and 30 ~ 100 nm wide) are observed. For pH = 7.5, the nanowires are straight with 60 nm diameter and a length > 1500 nm. The materials prepared at pH = 8.5 exhibit short-rod morphologies with a dimension of 130 ~ 160 nm in length and 20 ~ 30 nm in width. As for those prepared at pH = 9.5, short rods 80 ~ 100 nm in length and 20 ~ 50 nm in width can be observed. The influence of pH value on the interaction between surfactant molecules and reactant ions are responsible for these differences. In addition, the composition of the finial precipitation also depends on pH. Meanwhile, the ability to generate high axial ratio and well-crystallized nanowires, by coorganization of reverse micelles solutions and hydrothermal synthesis techniques, as described in this work, could offer an approach to the fabrication of one dimension nanomaterials.

Keywords nanoparticles, surfactant, reverse micelles, calcium phosphate, pH

Introduction

Calcium phosphate is an important biomaterial and the principal inorganic constituent of bones and teeth. Its formula is: $Ca_{10-x}(HPO_4)_x(PO_4)_{6-x}(OH)_{2-x}$ ($0 \leq \times \leq 2$). In this family, some compounds hold a particular position, hydroxyapatite (HA), with an atomic $Ca/P = 1.67$, is biocompatible and only slightly bioresorbable because of its insolubility. These properties, associated with those of osteoconduction, have led to it being used as a covering for prostheses. Monetite (dicalcium phosphate anhydrous, DCPA, $CaHPO_4$) is also worth paying attention to since it is also bioactive (1), simple to prepare (2) and found in small proportions in urinary (3) and dental stones (4). More recently, they have been investigated as protonic conductors (5, 6). The stability of calcium phosphates at ambient temperature and in aqueous solutions is determined by the pH value, as demonstrated by Driessens et al. (7). At pH values lower than 5, the

Received December 2005; Accepted April 2006.

Address correspondence to Chen Lai, Biomaterials Lab, College of Materials Science and Engineering, South China University of Technology, Guangzhou 510640, China. Fax: +86-20-85261559; E-mail: laichen1110@msn.com

most stable phase is dicalcium phosphate, monetite ($CaHPO_4$). At pH values between 5 and 9, octacalcium phosphate [$Ca_8(HPO_4)_2(PO_4)_4 \cdot 5H_2O$] or calcium-deficient hydroxyaptite [$Ca_{10}(PO_4)_6(OH)_2$,HA]. As for biomaterials, the morphology of calcium phosphate is of importance. because bone osteoblast cells (the cells that form new bone) are sensitive to the physical properties of their immediate surroundings, including surface composition, surface energy, roughness and topography (8). In addition, artifical bioceramics have always showed a lower tensile strength compared with natural bone (9), especially in an aqueous environment. This results in a strong limitation of the potential application of calcium phosphate ceramic as a replacement for heavy load-bearing bone. Fibers have generally exhibited high tensile properties because of their low dislocation density (10). With this view, one–dimensional nanomaterials of calcium phosphate have been synthesized recently for improving fracture toughness (11–13).

One promising route to control crystal size and shape is through confined synthesis from reagents dissolved in water-in-oil systems-reverse micelles solution. Reverse micelles have seen application in materials development, with many one-dimensional nanomaterials synthesized in reverse micelles, such as $BaSO_4$ (14), $BaCO_3$ (15), $CaSO_4$ (16), etc. Reverse micelles can be formed by ionic surfactants with long alkyl chains, such as cetyltrimethhylammonium bromide (CTAB) or by a mixture of ionic and nonionic surfactants with a short oxyethylene chain dissolved in organic solvents. Reversed micelles are usually thermodynamically stable mixtures of four components: surfactant, cosurfactant, organic solvent and water. Reverse micelles are a suitable reaction media for controlling the morphology of nanoparticles because water droplets can be seen as nanoreactors, favoring the formation of small crystallites with a sufficiently narrow size distribution (17, 18). The morphology of nanoparticles precipitated in reverse micelles can be markedly influenced by the nature of the surfactant and supramolecular architecture of the self-assembled aggregates (4). However, the products synthesized in reverse micelles at room temperature are often poorly crystalline and low yield with a long period. The hydrothermal synthesis can be carried out at a relatively low reaction temperature ($<250^\circ C$) to produce a sufficient high quality crystalline product without post-calcination. The solvothermal synthesis combines hydrothermal synthesis and reverse micelles solution, providing a unique approach for synthesis of nanomaterials (19, 20). In our previous papers, we described the solvothermal synthesis of needlelike, sheetlike and wire-like nanoparticles of calcium phosphate (21) and discussed the effects of the content of water and co-surfactant, reaction temperature, and ripening time (22) In the present paper, we focus on the influence of pH on the morphology and component of calcium phosphate.

Experimental

The materials used in our experiment were all analytical grade chemicals without further purification. The appropriate amount of cetyltrimethhylammonium bromide (CTAB), n-pentanol, reactant solution and cyclohexane were weighted into a glass vessel and stirred to a transparent isotropic solution. The characteristics of the microemulsion system used throughout the entire set of experiments were: $[CTAB] = 0.1$ M, $[\text{n-pentanol}]/[CTAB] = P_o = 3$, $[\text{water}]/[CTAB] = W_o = 10$, $[Ca(NO_3)_2] = 1$ M and $[H_3PO_4] = 0.5$ M. PH value was adjusted by $NH_3 \cdot H_2O$. The resulting solution was then transferred into a sealed Teflon container and statically heated in a $100^\circ C$ furnace for 10 h. The products were washed several times with ethanol and ether. Finally the white sample was dried at $50^\circ C$ in an oven.

Morphology of the as-synthesized powders, which were dispersed in ethanol, was characterized by TEM (PHILIPS CM300), using an accelerating voltage of 200 kV. The phase composition and crystallinity of the powders were analyzed by X-ray diffraction (XRD) using a Brüker AXS, D8 Advance Diffractometer with Cu K_α radiation at 40 kV and 40 mA. Fourier transform infrared absorption spectra (FTIR) were obtained by using Nicolet Nexus FT-IR equipment.

Results and Discussion

The XRD patterns of calcium phosphate synthesized with different pH value, which is varied from 6 to 9.5, are shown in Figure 1. At pH = 6.0, the product consisted of monetite ($CaHPO_4$, DCPA) and HA (Figure 1a). Increasing the pH to 7.5 and 8.5

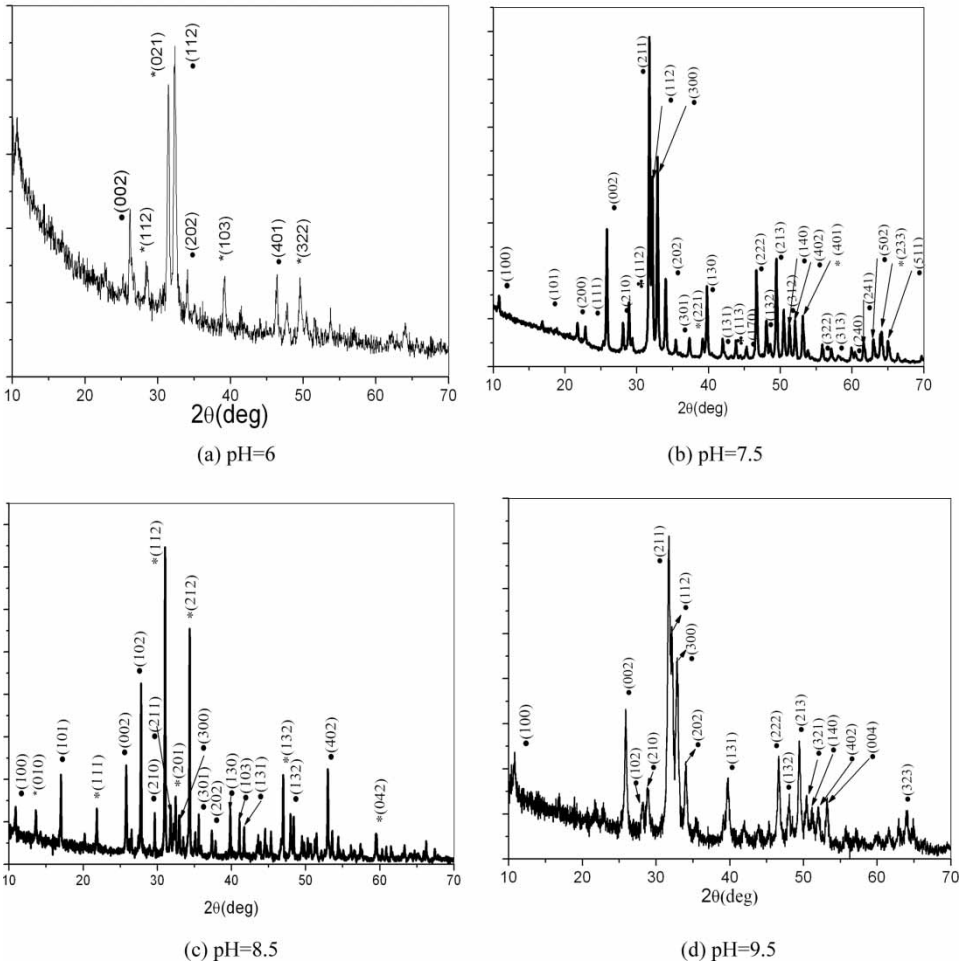

Figure 1. XRD patterns of calcium phosphate nanowires prepared at $W_o = 10$, $P_o = 3$ but at different pH values: (a) pH = 6; (b) pH = 7.5; (c) pH = 8.5; (d) pH = 9.5 demonstrating the structural transformation from $CaHPO_4$ (DCPA) to $Ca_{10}(PO_4)_6(OH)_2$ (HA).

results in the appearance of a more HA phase (Figure 1b), coexisting with several peaks of DCPA. Upon increasing the pH to 9.5, the dominant phase is HA, and the DCPA phase is the very minor phase (Figure 1c). The latter indicates that $CaHPO_4$ gradually gets transformed into HA under higher pH value according to the following reaction (23):

$$10CaHPO_4 + 2H_2O \longrightarrow Ca_{10}(PO_4)_6(OH)_2 + 4H_3PO_4$$

Figure 2 shows the FTIR spectra of as-prepared calcium phosphate at different pH values. The absorption bands at 1128–1015 cm^{-1} and 573–513 cm^{-1} are attributed to $\upsilon_3PO_4^{3-}$ and$\upsilon_4PO_4^{3-}$, respectively. Bands appearing at wave number values of 897 and 1399 cm^{-1} are indicative of the carbonate ion substitution (24). Some researchers considered it as coming from a reaction between atmospheric carbon dioxide (25). One may expect an increase in carbonate concentrations at an increasing pH value. We also detect the band at 2358 cm^{-1} for soluble CO_2 (g) in the calcium phosphate materials. All these might be due to a change in crystallinity and/or distortion of symmetry caused by the insertion/rearrangment of various foreign impurities with a progressive increase in pH value (26). In addition, some bands show the presence of organic materials (2900 cm^{-1} for C-H vibration bands), indicating that CTAB is therefore incorporated into the calcium phosphate during the preparation.

It is generally accepted that the peak intensity and sharpness of $\upsilon_3po_4^{3-}$ absorption bands are indications of the degree of crystallinity (23, 27–31). The splitting factor (sf) defined by Weiner and Bar-Yosef has become the dominant crystallinity measure in archaeology (28, 29). SF is calculated by summing the heights of the 563 and 603 cm^{-1} peaks and dividing this value by the height of the trough between them as shown

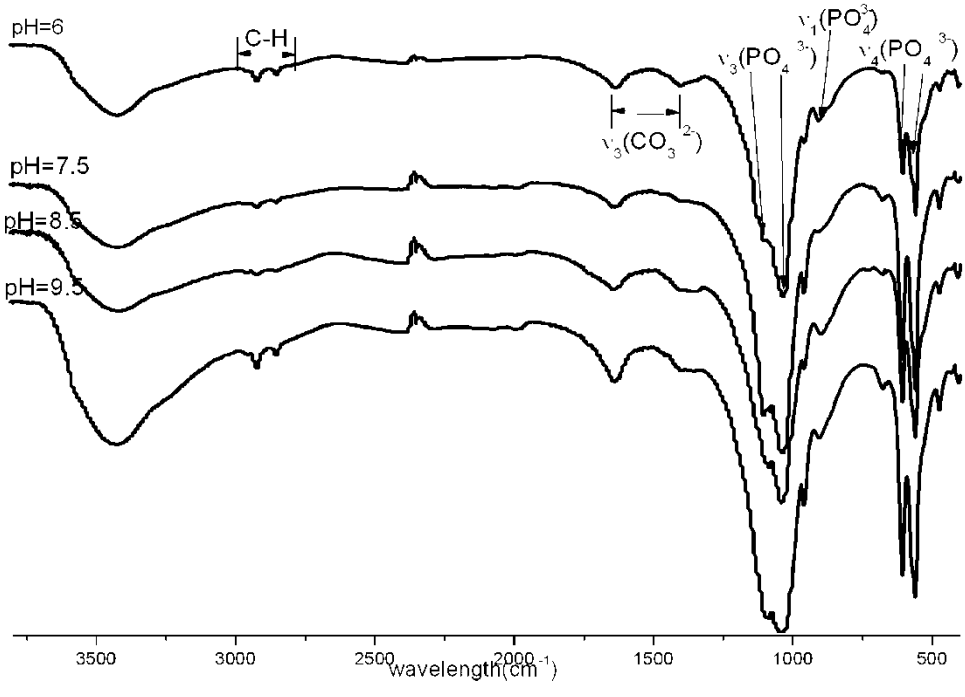

Figure 2. FTIR spectra of calcium phosphate synthesized at different pH value.

in Figure 3. The double peaks become increasingly separated, or split, as crystallinity increases. Figure 4 shows the variation in SF vs. Ph value, suggesting that the products become morewell-crystallized with the increasing of ph value.

Figure 5 shows the TEM images of calcium phosphate nanoparticles prepared at different pH. All the samples synthesized by solvothermal method exhibit one-dimensional morphologies. At pH $\leq$ 6, long nanowires, 800 nm long and 30 $\sim$ 100 nm wide, are observed by electron microscopy (Figure 6a). For pH = 7.5, the nanowires are straight with diameter in 60 nm and length more than 1500 nm (Figure 5b). The materials prepared at pH = 8.5 exhibit short-rod morphologies (Figure 5c) with dimension of 130 $\sim$ 160 nm length and 20 $\sim$ 30 nm width. As for those prepared at pH = 9.5, nanoparticles with 80 $\sim$ 100 nm in length and 20 $\sim$ 50 nm in width can be observed (Figure 5d). These particles all have curved and round edges, indicating that these nanowires or nanorods have not been broken by electron bean illumination during TEM observation. It can also be observed that the particles formed at pH = 8.5 are larger than those formed in a pH = 9.5 system.

From the results given above, it is obvious that pH can have a dramatic effect on the composition, crystallinity and morphology of calcium phosphate. The effects of pH on the HA crystallization in the present of surfactant can be interpreted in terms of the influence of pH on the interaction between the ionized head groups of

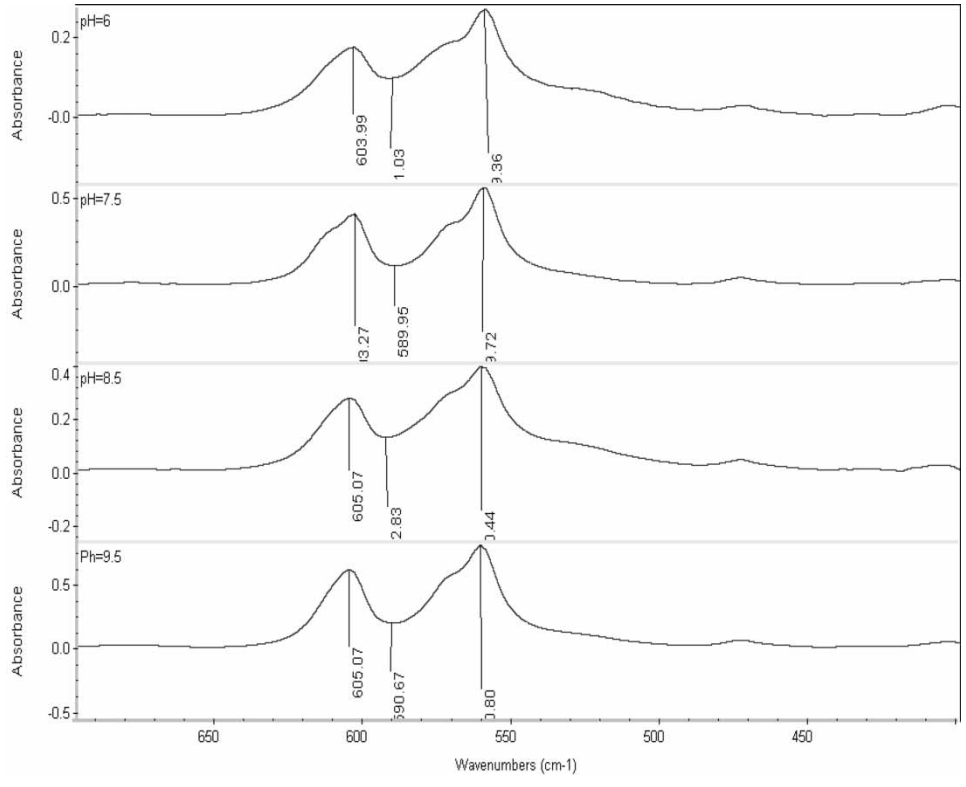

Figure 3. Splitting function (SF) of Weiner & Bar-Yosef. SF is measured as the sum of the heights of the 603 and 563 cm^{-1} phosphate peaks divided by the height of trough between them. All heights are measured above a baseline draw from approximately 607 to 495 cm^{-1}.

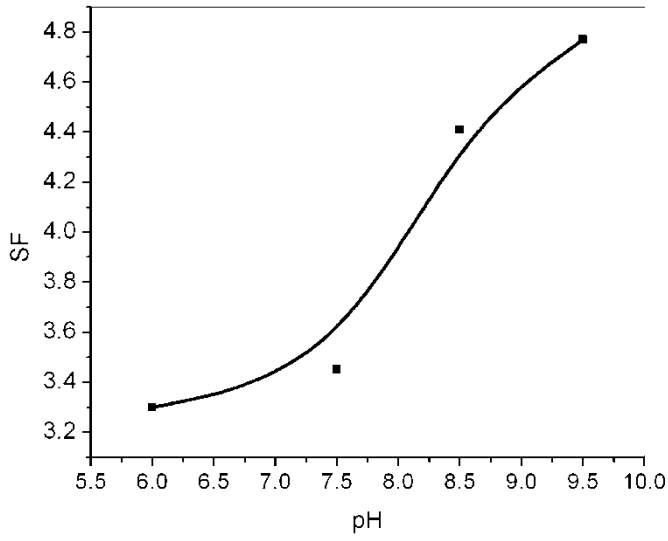

Figure 4. Variation in SF vs pH value.

the cation surfactant and reactant ions. As for cation surfactant, CTAB ionized completely in the water phase and results in a cation CTA^+ with tetrahedral structure. Meanwhile, phosphate anion is also a tetrahedral structure (11). Thus, the production of calcium phosphate crystallized solid would be due to CTAB molecule pre-organization at the oil/water interface (Figure 6). Because of their affinity for CTA^+ ions, PO_4^{3-} ions are immobilization at the oil/water interface and follow the geometry dictated by the association of surfactant molecules. During the addition of Ca^{2+} solution, PO_4^{3-} ions bind simultaneously to the surfactant molecule and Ca^{2+}. Their outcome is oriented calcium phosphate nucleation on the support composed of the organized CTAB molecules. However, with pH $>$ 7.5, the reverse micelles solution is observed to turn a bit hazy in our experiments, indicating fluctuations and destabilization of the reverse micelles. It can be speculated that with pH $>$7.5, ionized CTA^+ headgroups prefer to interact with OH^- ions which are present from the ammonia addition. Therefore, a large inhibition effect on the HA crystallization occurs due to the interaction between CTA^+ and OH^-. Meanwhile, the surfactant molecules are excluded from the crystallization surfaces as the calcium phosphate nucleus grows gradually, leading to the invalidation in the growth guiding role of CTAB on the crystallization of calcium phosphate. Under such unstable conditions, the formation of a larger size crystallite are not favored. The TEM studies in Figure 5b, c and d show the significant decrease in the axial ratio of calcium phosphate particles with increasing pH from 7.5 to 9.5, corroborating our above mentioned assumption. Addition of ammonia to the reverse micelles solution results in the bulk precipitation of one-dimensional crystals with a small aspect ratio, suggesting that the association between the ionized CTAB and the precipitated calcium phosphate is weak, even though a high PO_4^{3-} ion binding capacity might be expected under conditions where most of the headgroups of CTAB are protonated.

Compared to those at pH $>$ 7,calcium phosphate particles which grow at lower pH, such as 6–7, have undergone a different growth process. Here, surfactant molecules

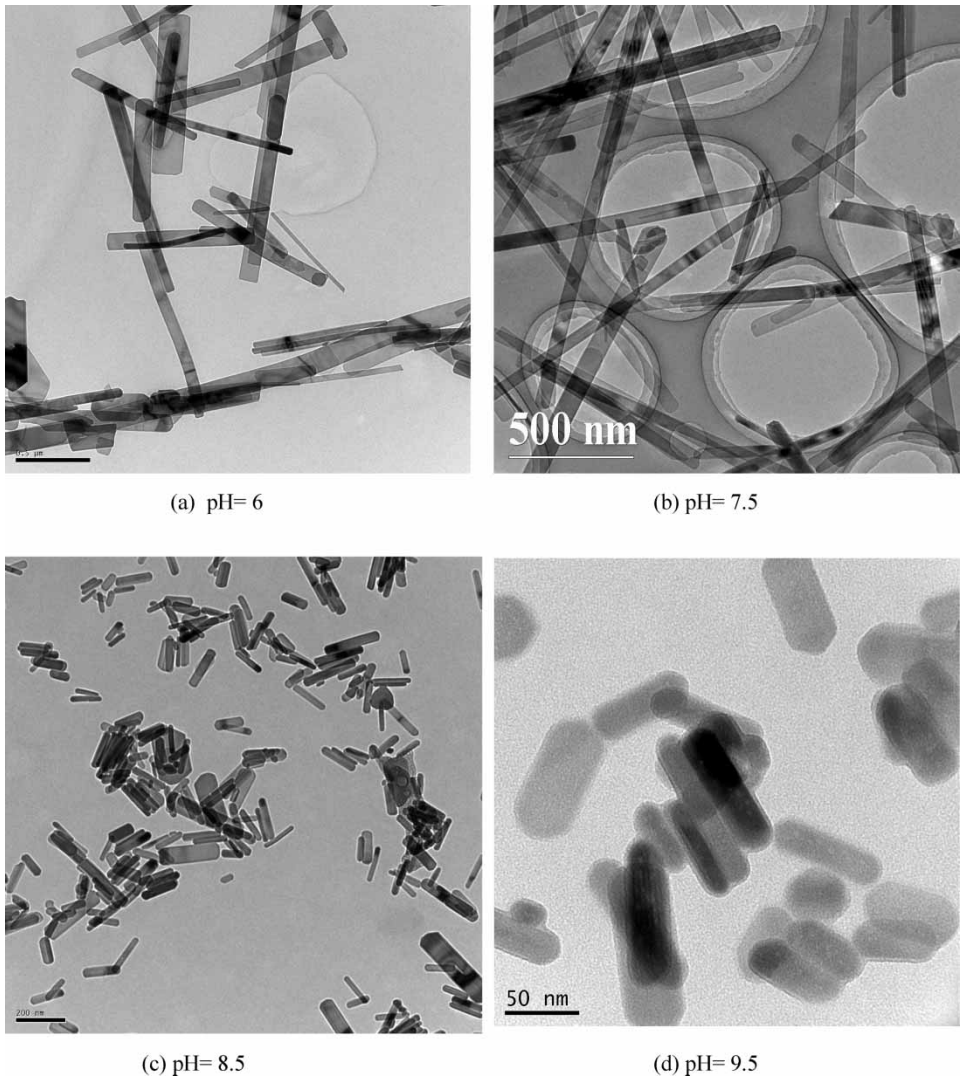

(a) pH= 6 (b) pH= 7.5

(c) pH= 8.5 (d) pH= 9.5

Figure 5. TEM micrograph of powders prepared at different pH value.

exposed to PO_4^{3-} ions dominate, resulting in an interaction between the CTA^+ and the growing calcium phosphate nucleus, and thus oriented calcium phosphate nucleation on the HA crystallization is found. As for the CTAB reverse micelles, several researchers (32) have shown that they form wormlike aggregations in solution. Under this condition, the growth of calcium phosphate prefers to copy their template's shape, resulting in the formation of nanowires with high axial ratio as shown in Figure 5a and b. As we described above, DCPA transform into HA as pH value increases. Tablet form is the preferred crystal habit of $CaHPO_4$ (33), while needle formation is rather a generic feature of HA (34). As a result, the axial ratio of the calcium phosphate complex, prepared at pH = 6.0–7.5, increases when larger amount of HA appears in the products.

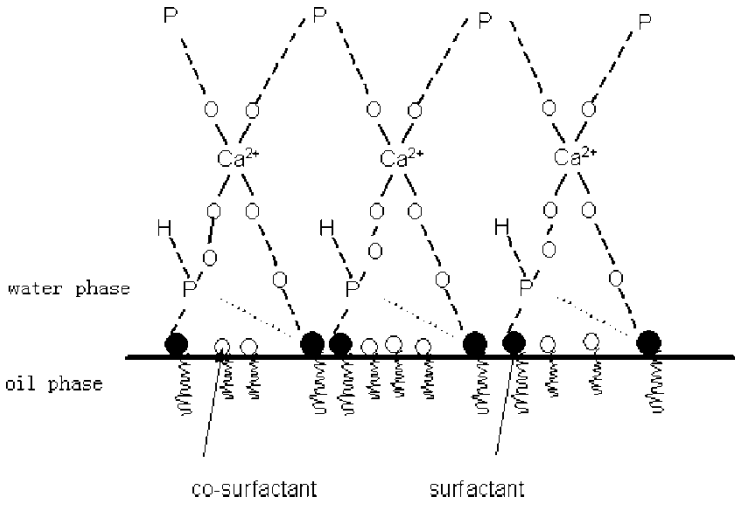

Figure 6. Model of oriented crystallization of calcium phosphate in the presence of CTAB.

The results in our experiments are hard to reconcile with the results that hydroxyapatite is the main produce when PH values are above 4.2 (35). This might be due to the fact that HA would like to expose the Ca^{2+} cations but not the PO_4^{3-} anions at all faces except (001) (34), as shown in Figure 7. But in our experiment, the reverse micelles solution consisted of the cations surfactant CTAB which interacted with PO_4^{3-} preferentially, leading to easily exposing the PO_4^{3-}. Therefore, under this temperature, many $CaHPO_4$ are turned into HA with enough OH^- in the basic solution and crystal nuclei formed in the bulk solution. Consequentially, HA is deposited without the selective adsorption of CTA^+. It is worth mentioning that solvothermal reactions have been performed in the sealed and opaque Teflon autoclave. Thus, the invisible reaction process makes the growth mechanism of nanowires at higher temperature ambiguous. Therefore, the reverse micelles likely plays a major role in the very early stage of crystal growth at room temperature.

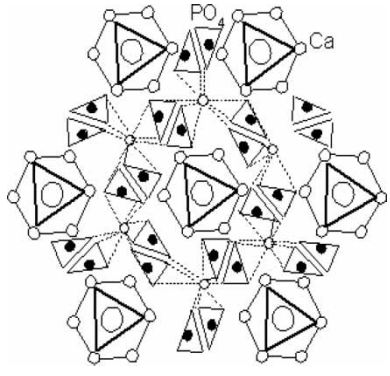

Figure 7. Hydroxyapatite crystal structure along the crystal *c*-axis.

Conclusion

One dimensional calcium phosphatem nanomaterials are synthesized by a solvothermal method at 100°C for 10 h in a CTAB reverse solution. The pH value has great influence on the crystal component and morphology. At lower pH value of 7.5 and 6, nanowires with high axial ratio can be obtained. In contrast, only short-rod nanoparticles can be produced at higher pH. With increasing pH, the crystallinity of products increase. In our experiment, CTAB plays the role of guiding crystal growth at the very early stage of crystal growth at room temperature. Higher pH results in weakening interactions between the amino group of CTAB and the reactant PO_4^{3-}, leading to crystal nucleating in the bulk water phase without the growth-guiding of surfactant molecules. The XRD patterns reveal the coexistence of two phase HA and $CaHPO_4$. Due to the selective adsorption of ionized amino groups on the surfactant, $CaHPO_4$ is the more favorable product.

Acknowledgments

This work was supported by the National Nature Science Foundation of China (59932050, 50272021 and 50472054), the Foundation of the State Key Developing Plan for Fundamental Research (973 Plan) of China (2005CB623902) and the China postdoctoral Science Foundation (2004036496).

References

1. Oonishi, H., Hench, L.L., Wilson, J., Sugihara, F., Tsuji, E., Kushitani, S., and Iwaki, H.J. (1999) *Biomed. Matt. Res.*, 44 (1): 31–43.
2. Jinawath, S. and Sujaridworakun, P. (2002) *Mater. Sci. Eng. C*, C22 (1): 41–46.
3. Daudon, M., Donsimoni, R., Hennequin, C., Fellahi, S., Le Moel, G., Paris, S., Troupel, M., and Lacour, B. (1995) *Urol. Res.*, 23 (5): 319–327.
4. Werness, P.G., Bergert, J.H., and Smith, L.H. (1981) *J. Cryst. Growth*, 53 (5): 166–181.
5. Tortet, L., Gavarri, J.R., Nihoul, G., and Dianoux, J. (1997) *Solid State Ionic*, 97 (1): 253–256.
6. Tortet, L., Gavarri, J.R., and Nihoul, G. (1997) *J. Solid. State. Chem.*, 132 (1): 6–16.
7. Rudolph, P. and Fukuda, T. (1999) *Cryst. Res. Tech.*, 34 (1): 3–40.
8. Shwartz, Z., Lohmann, C.H., and Oefinger, J. (1999) *Adv. Dent. Res.*, 13 (1): 38–48.
9. Hench, L.L. (1991) *J. Am. Ceram. Soc.*, 74 (7): 1487–1510.
10. Laudise, R.A. (1970) *Growth of Single Crystals*; Prentice-Hall, Inc: New Jersey.
11. Yan, L., Li, Y.D., Deng, Z.X., Zhuang, J., and Sun, S.M. (2001) *Inter. J. Inorganic. Mater.*, 3 (7): 633–637.
12. Kolos, E., Ruy, A., and Roger, G. (2003) *Key. Eng. Mater.*, 240–242): 47–50.
13. Liou, S.C., Chen, S.Y., and Liu, D.M. (2003) *Biomaterials*, 24 (22): 3981–3988.
14. Hopwood, J.D. and Mann, S. (1997) *Chem. Mater.*, 9 (8): 1819–1828.
15. Kuang, D.B., Xu, A.W., and Fang, Y.P. (2002) *J. Cryst. Growth*, 244 (2–3): 379–383.
16. Rees, G.D., Evans-Gowing, R., and Hammond, S.J. (1999) *Langmuir*, 15 (6): 1993–2002.
17. Sato, H., Hirai, T., and Komasawa, I. (1995) *Ind. Eng. Chem. Res.*, 34 (7): 2493–2498.
18. Pileni, M.P. (1997) *Langmuir*, 13 (13): 3266–3276.
19. Yang, J., Zeng, J.Y., Yu, S.H., Yang, L., Zhou, G., and Qian, Y.T. (2000) *Chem. Mater.*, 12 (11): 3259–3263.
20. Yu, S.H., Yang, J., Han, A.H., Zhou, Y., Yang, R.Y., Xie, Y., Qian, Y.T., and Zhang, Y.H. (1999) *J. Mater. Chem.*, 9 (6): 1283–1287.
21. Lai, C., Tang, S.Q., Wang, Y.J., and Wei, K. (2005) *Mater. Lett.*, 59 (2-3): 210–214.
22. Wang, Y.J., Lai, C., Wei, K., and Tang, S.Q. (2005) *Mater. Lett.*, 59 (8-9): 1098–1104.
23. Perloff, A and Posner, A.S. (1956) *Science*, 124 (3222): 583–584.

24. Stoch, A., Jastrzebski, Brozek, W., Stoch, J., Szaraniec, J., Trybalska, B., and Kmita, G. (2000) *J. Mol. Struct.*, 555 (1): 375–382.
25. Sonoda, K., Furuzono, T., Walsh, D., Sato, K., and Tanaka, J. (2002) *Solid State Ionics.*, 151 (1-4): 321–327.
26. Panda, R.N., Hsieh, M.F., Chung, R.J., and Chin, T.S. (2003) *J. Phys. Chem. Solid*, 64 (2): 193–197.
27. Pleshko, N., Boskey, A., and Mendelsohn, R. (1991) *Biophys. J.*, 60 (4): 786–793.
28. Weiner, S. and Bar-Yosef, O. (1990) *J. Arch. Science*, 17 (2): 187–196.
29. Weiner, S., Goldberg, P., and Bar-Yosef, O. (1993) *J. Arch. Science*, 20 (5): 613–627.
30. Wright, L.E. and Schwarcz, H.P. (1996) *J. Arch. Science*, 23 (6): 933–944.
31. Surovell, T.A. and Stiner, M.C. (2001) *J. Arch. Science*, 28 (6): 633–642.
32. Törnblom, M. and Henriksson, U. (1997) *J. Phys. Chem. B*, 101 (31): 6028–6035.
33. Jinawath, S., Polchai, D., and Yoshimura, M. (2002) *Mater. Sci. Eng. C*, 22 (1): 35–39.
34. Peytcheva, A., Cölfen, H., Schnablegger, H., and Antoniette, M. (2002) *Colloid. Polym. Sci.*, 280 (3): 218–227.
35. Hohl, H., Koutsoks, P.G., and Nancollas, G.H. (1982) *J. Cryst. Growth*, 57 (2): 325–335.